Predicting aromatic exciplex fluorescence emission energies

Journal:	*Physical Chemistry Chemical Physics*
Manuscript ID	CP-ART-04-2019-002027.R1
Article Type:	Paper
Date Submitted by the Author:	02-May-2019
Complete List of Authors:	Krueger, Rachel; Caltech, Chemistry Blanquart, Guillaume; Caltech, Mechanical and Civil Engineering

PCCP

ARTICLE TYPE

Cite this: DOI: 00.0000/xxxxxxxxxx

Predicting aromatic exciplex fluorescence emission energies†

Rachel A. Krueger,*[a] and Guillaume Blanquart,[b‡]

Received Date
Accepted Date

DOI: 00.0000/xxxxxxxxxx

PAH dimerization has been widely posited to play an important, even rate-determining role in soot nucleation, despite scanty experimental evidence of the existence of PAH dimers in flames. Laser-induced fluorescence (LIF) offers a promising *in situ* method of identifying PAH dimers, if dimer fluorescence can be distinguished from the fluorescence of the constituent monomers and other species present. Predicting transition energies for excited dimers (excimers) and excited complexes (exciplexes) represents a significant challenge for theory. Nonempirically tuned LC-BLYP functionals have been used to compute excited-state geometries and emission energies for a database of 81 inter- and intramolecular PAH excimers and exciplexes. Exciplex emission energies depend sensitively on the topology of the PAHs involved, but a linear relationship between the mean monomer bandgap and the computed exciplex emission means that dimer electronic properties can be predicted based on the properties of the constituent monomers. The range of fluorescence energies calculated for structures containing small to moderately-sized PAHs indicates that either noncovalent or aliphatically-linked complexes could generate the visible-range fluorescence energies observed in LIF experiments.

1 Introduction

The negative effects of soot on human health[1,2] and earth's climate[3,4] are well-known, but efforts to develop predictive, transferable soot formation models are hampered by uncertainty about the molecular mechanism of soot nucleation and growth. Polycyclic aromatic hydrocarbons (PAHs) are relatively stable at flame temperature,[5] and many have sizes consistent with the molecules observed in electron microscopy images of nascent soot particles.[6] These observations have led many to favor PAHs as the building blocks of soot nuclei, with the initial PAHs either connected by covalent bonds or held together by dispersion interactions.[7] However, direct experimental evidence of the existence of covalent or noncovalent PAH complexes in flames is scarce, and noncovalent cluster nucleation has not been observed for moderately-sized PAHs in molecular dynamics simulations of pure PAH gases.[8–10]

A range of recently-developed *in situ* experimental techniques have the potential to provide a more complete census of the species present in flames.[11] Absorption measurements[12] and laser-induced fluorescence (LIF) studies[13] provide a window into the electronic properties of hydrocarbons in flames. Resolving LIF spectra in terms of height above the burner (HAB) demonstrates how these electronic properties change as HAB increases, temperature decreases, and the balance of chemical reactions shifts. Below 15 mm HAB, UV excitation results in the UV-range emission characteristic of small PAH monomers such as naphthalene and pyrene. At larger HAB, though, a distinct visible-range emission of $\geq$ 500 nm (20000 cm^{-1}) is observed, well below the emission energies of the largest PAHs that are kinetically favored to form in flames.[13]

This red-shifted signal, a known spectroscopic feature of flames,[14] is consistent with the formation of PAH excimers.[13] Excimer ("excited dimer") formation occurs when an electron-hole pair becomes delocalized over neighboring chromophores, stabilizing the intermolecular interaction through a mixture of exciton resonance and charge resonance. The initial photoabsorption event often involves a single molecule, so absorption spectra may not be affected.[15] When the two chromophores are not identical, the term exciplex ("excited complex") is used.

Exciplex formation is known to play an important role in the photophysics and photochemistry of many systems containing aggregates of chromophores, from DNA[16] to organic photovoltaics.[17,18] The strength of the exciplex interaction is proportional to the orbital overlap of the two molecules, which decreases exponentially with increasing internuclear distance. Thus, an observ-

[a] 1200 E. California Blvd., MC 104-44, PASADENA, CA, USA.
[b] 1200 E. California Blvd., MC 104-44, PASADENA, CA, USA. Fax: 626 568 2719; Tel: 1 626 395 4306; E-mail: g.blanquart@caltech.edu

† Electronic Supplementary Information (ESI) available: comparison of LC-BLYP-T and B2PLYP-D3 fluorescence energies, noncovalent dimer configurations, range-split parameters, oscillator strengths, and Cartesian coordinates for optimized excited-state structures. See DOI: 10.1039/b000000x/

able exciplex emission in flames indicates the presence of PAHs in close proximity to one another—the optimal intermolecular distances for S_1 excimers and exciplexes of small acenes range from $\approx$ 3.0–3.3 Å.[19–22]

Considering excimer emissions from three to five noncovalent PAH homodimers may be sufficient to model the observed visible-range emission,[13] but if these homodimers are present in flames, it is likely that many others are as well. Further, the number of possible PAH heterodimers that can form from a given population of PAHs far exceeds the number of homodimers. Theoretical studies of PAH complex electronic structure have so far been limited to homodimers of PAHs the size of pyrene or smaller[19,22–26] or have focused on the complex HOMO-LUMO gap, a quantity related to the complex absorption energy but not an experimental observable.[27]

Our first objective for this work is to provide a database of high-quality time-dependent density functional theory (TDDFT) fluorescence emission energies for noncovalent PAH homo- and heterodimers, focusing on complexes containing the small- and medium-sized PAHs likely to be present in the largest quantities in flames. These PAHs have recently been identified as the most probable soot-nucleating species.[28] The S_1 transition is chosen because, for most PAHs, Kasha's rule states that fast internal conversion leads to emission from the lowest-energy singlet state.[29] Ultimately, calculating fluorescence emission energies for every possible heterodimer is not a computationally tractable approach, so we will attempt to link calculated exciplex fluorescence for the heterodimers with the electronic and geometric properties of the constituent monomers. If such relationships exist, they will allow spectroscopists to make use of the large databases of calculated PAH monomer properties already available.[30,31]

To simplify this analysis, three subsets of complexes will be considered in turn. The first consists of excimers made up of the isomers of tetracene; the arrangement of the aromatic rings represents the only degree of freedom in this subset. Excimers of pentacene isomers will be considered separately for the same reason, despite limited relevance in flame environments. Slow PAH growth kinetics will limit the concentration of such large species in flames,[7] and pentacene is unstable even in ambient-temperature air.[32] Next, we will consider a mix of homo- and heterodimers containing naphthalene, allowing the mass and geometry of the other monomer to vary. Trends observed in each subset will provide a lens for analyzing the entire database.

Finally, it is important to consider the possibility that visible-range fluorescence may be generated by covalently-linked PAHs. Covalent bond formation between relatively small unsaturated species, possibly including barrierless reactions that involve resonance-stabilized radicals,[33] has been included in recent soot-formation mechanisms.[28] Mass spectrometry results point to the presence of a population of moderately-sized, aliphatically-bridged PAHs.[34] This is why the final objective is to calculate fluorescence emission energies for a representative collection of PAH complexes connected by covalent linkers with varying lengths and connection points to determine how aliphatic linkers impact the electronic properties of complexes.

2 Methods

Describing the lowest-energy singlet valence excited states of PAHs represents a well-known challenge for DFT. The electronic structure of acene monomers is marked by two low-lying singlet excited states. The L_a state consists almost entirely of a HOMO→LUMO transition, while the L_b state represents a mix of HOMO-1→LUMO and HOMO→LUMO+1 transitions. Noncovalent dimer formation can change the energy ordering of the transitions; e.g., the L_b state is lower in energy than the L_a state for the naphthalene monomer, but the order is reversed for the dimer, with the state energies crossing around an intermolecular distance of 3.5 Å.[19,35] Several hybrid functionals, including the popular B3LYP functional, reverse the order of these states for the naphthalene monomer.[36,37] The LC-BLYP functional[38] provides a reasonably well-balanced treatment of the L_a and L_b excitations in acenes. This range-separated functional also reproduces the short-range attractive portion of the acene exciplex potential energy surfaces (around 3 Å) without an additional dispersion correction.[20]

Performance of the LC-BLYP functional may be further optimized by tuning the range-split parameter γ, which controls the switching between DFT exchange at short interaction distances and Hartree-Fock exchange at long interaction distances.[39,40] For each starting structure, γ is chosen to minimize the disagreement between calculated orbital energies for the neutral and ionized structures and the predictions made using the DFT version of Koopman's theorem. The tuning procedure improves the description of the exciplex interaction around the minimum-energy geometry without significantly changing monomer excitation energies, leading to better agreement between DFT and multireference exciplex binding energies.[20] Values of γ used for each complex and monomer are reported in Tables S1-S4. As a check, fluorescence energies have been recalculated for a subset of complexes using the B2PLYP functional[41] with doubles correction,[42] which has also been shown to describe exciplex interactions well.[20] The two functionals are in good agreement, with the B2PLYP functional predicting emission energies slightly lower than the tuned LC-BLYP functional for most complexes (Fig. S1).

Calculating oscillator strengths for electronic transitions is an important second step in estimating their contributions to experimental spectra and predicting relative fluorescence band intensity. Range-separated functionals in general reproduce EOM-CCSD oscillator better than either GGA or hybrid GGA functionals, with the LC-BLYP functional among the top three performers.[43] The tuned LC-BLYP functional has also shown top performance for calculated fluorescence lifetimes.[44]

Tuned versions of the LC-BLYP functional (LC-BLYP-T) have been used in all electronic transition energies and oscillator strengths reported, and LC-BLYP-T analytical gradients were used in the S_1 potential energy surface geometry optimization. The def2-TZVP basis set[45] was chosen because it yields electronic transition energies that agree well with the ones calculated using the much larger aug-cc-pVTZ basis set,[46] and def2-TZVP binding energies for small exciplexes are in good agreement with multireference results.[20] Basis set error in multireference calculations

of exciplex binding energies has been discussed extensively in a recent work.[21] The Tamm-Dancoff approximation was applied. Calculations were carried out using the ORCA electronic structure package[47] version 4.0.0. Integration grid size 5 was used, with tight SCF convergence.

Eclipsed configurations typically represent the lowest-energy geometry for aromatic excimers,[48–50] so starting structures for the exciplexes were chosen to maximize the number of overlapping aromatic rings. An initial intermolecular separation of 3.3 Å was chosen based on previously-calculated optimal exciplex separations.[20] The fluorescence emission energy ΔE_F represents the vertical transition energy at the minimum-energy geometry on the S_1 potential energy surface. The energy difference between ΔE_F and the monomer absorption energy ΔE_A represents the sum of the exciplex binding energy and the energy difference on the ground-state potential energy surface between the optimal ground-state geometry and the optimal S_1 geometry, often referred to as the repulsion energy. Coordinates for the minimum-energy S_1 structures are reported in Supplementary Information. The monomer bandgap or optical gap for monomers is calculated as the difference between the highest-occupied and lowest-unoccupied orbital energies (ΔE_{HL}) at the optimal ground state geometry, as recorded in the PAH Index.[51]

3 Results and Discussion

3.1 Tetracene Isomer Excimers.

We begin our survey with an examination of homodimers composed of tetracene isomers, where molecular geometry represents the only degree of freedom. Electronic properties of each monomer are reported in Table 1, along with the shortened names that will be used in this work. Representative Clar structures[52] for each tetracene monomer, and the other PAH monomers considered, are illustrated in Fig. 1.

A strong stabilizing excimer interaction is observed for all of the isomers, corresponding to red shifts of about 30000-40000 cm^{-1} (Table 2). For four of the isomers, an almost perfectly linear relationship exists between ΔE_F for the excimer and ΔE_{HL} for the monomer (Fig. 2a). Replacing ΔE_{HL} with the ΔE_F values computed for the monomers yields another clearly linear relationship, albeit one with reduced explanatory power; the amount of variation in ΔE_F for the excimers explained by variation in monomer ΔE_F values is 85%, compared with 97% for ΔE_{HL} (Table 3).

The benzo exciplex emission energy is elevated relative to the chrys emission energy, despite a very similar ΔE_{HL}. This distinctive behavior may well stem from the geometric differences—the benzo monomer has a u-shape, and the molecule is bent to prevent steric clashes between hydrogen atoms. Dihedral angles within the curve of the u are -13.2° and 15.6°, values that remain nearly identical upon excimer formation. The deviation of each monomer within the relaxed excimer from perfectly planar geometry may be quantified using the planarity index, a measure based on the mean distance of atoms from a three-atom plane within the molecule, using the plane that minimizes this distance. A planarity index of 0 indicates a planar molecule.[53]

Benzo has by far the largest planarity index (Table 2), a level of distortion that contributes to large intermolecular distances between overlapping carbons in the excimer structure. C-C distances range from 3.24-3.96 Å, compared with 3.08-3.60 Å for chrysene. Because the strength of the exciplex interaction depends on orbital overlap, which decays exponentially with internuclear separation, differences in intermolecular C-C distances of approximately 0.3 Å can have a noticeable impact on exciplex stabilization. The lack of frontier orbital electron density in the intermolecular region of the benzo excimer(Fig. 3a) compared with, for example, the tet excimer (Fig. 3b) is apparent. Monomers of the other tet isomers are also nonplanar in the minimum-energy excimer structure, but shorter C-C distances are maintained (3.18-3.54 Å for tet and 3.02-3.76 Å for benza).

The ordering of ΔE_{HL} energies in tet isomers is well-known, and has been rationalized using the PAH's Clar structures (Fig. 1).[30] Clar structures are generated by placing benzene-like aromatic sextets (denoted by circles) in PAH rings and adding the remaining π electrons as double bonds. One aromatic sextet may be placed in each acene-like row of adjacent rings. Rings containing aromatic sextets are regarded as having higher local aromaticity. Large proportions of aromatic sextets and single bonds are associated with high ΔE_{HL} values, which generally correspond to higher thermodynamic and kinetic stability.[52] Among the tet isomers, the only possible Clar structure for tri displays both of these characteristics, and indeed tri has the highest ΔE_{HL} value of the isomers, while tet, with a single aromatic sextet and a number of double bonds, has the lowest.

For $C_{32}H_{16}$ PAHs, ΔE_{HL} has been shown to increase with the number of aromatic sextets, but the predictive value of sextet count alone is limited; for a given sextet number, ΔE_{HL} values vary by 1600–9700 cm^{-1}.[30] Three of the tet isomers have a sextet count of two. Quantitative descriptions of PAH edges offers another route to characterizing PAH topology. Mosbach and coworkers identify four types of PAH edge sites (Fig. 4).[54]

To obtain a one-dimensional ΔE_F model, we focus on a single edge type: zig-zag sites. Zig-zag sites are found along the central edges of linear acenes, distinct from the free edges found on both ends. The number of bonds that are part of zig-zag sites, N_Z, is different for each tet isomer, with the linear tet isomer having the maximum possible N_Z and the tri isomer having none. The N_Z value calculated for each excimer includes the number of zig-zag bonds present in both excimers. Emission energies from four of the excimers display a clear linear relationship with the number of zigzags (Fig. 2b), but the emission energy of benzo is again somewhat elevated as a result of the distortion caused by the bay edge group formed by the inside edge of the u.

Linear acenes also have the largest possible intramolecular C-C distances. We define the diameter D of a molecule to be the maximum intramolecular C-C distance and find a similar linear relationship between D and ΔE_F. N_Z slightly outperforms D as a predictor of ΔE_F, but the R^2 values obtained for each are similar.

Mean C-C bond length represents another structural feature correlated with aromaticity.[55] Here we use mean excited-state monomer bond length, which cannot be determined *a priori* like sextet number and requires a structure optimized in the excited state. Because this structure is the monomer, the resources re-

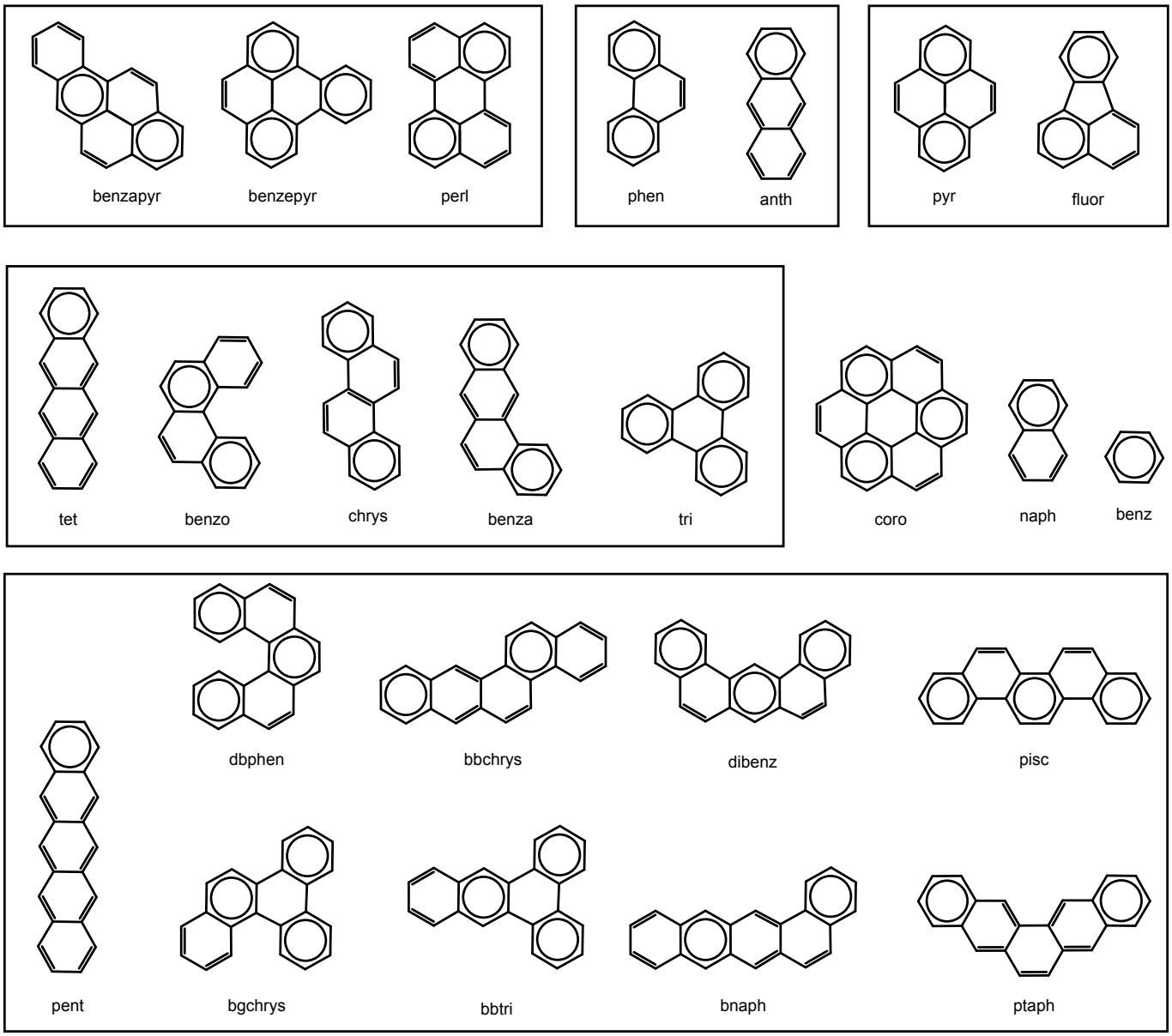

Fig. 1 Clar structures[52] for the PAH monomers considered in this work. In each case, a representative Clar structure is shown, although multiple distributions of aromatic sextets may contribute to the overall electron density. Isomers are shown in the same box.

quired to calculate $\overline{r_{CC}}$ are significantly smaller than those required for the complex ΔE_F calculation. The correlation coefficient R^2 obtained from the linear fit of ΔE_F with respect to $\overline{r_{CC}}$ (Fig. 2c) indicates that 99% of the variation in ΔE_F may be explained by its relationship with $\overline{r_{CC}}$ (Table 3), making it the most successful single geometry descriptor. Substituting mean ground-state bond length decreases R^2 to 0.03, underlining the significant differences in geometry and aromaticity between the two states.

3.2 Pentacene Isomer Excimers.

To extend our exploration of topology effects on ΔE_F, we have considered a representative subset of the 12 isomers of pentacene. The linear relationship between ΔE_F and ΔE_{HL} is clear (Fig. 5a), and for pentacene, ΔE_{HL} is the most accurate predictor of ΔE_F. The ordering obtained for monomer ΔE_{HL} is in good agreement with recent TDDFT results.[56] Again, ΔE_{HL} performs better than ΔE_F for the monomer as a predictor of excimer emission energy (Table 3).

For the geometric descriptors, though, the picture becomes more complicated. Several of the isomers have bay edge groups, but the location of the bay is important in determining the S_1 excimer geometry. Bnaph and bbchrys each have a single edge group and nonplanar monomers—intermolecular C-C distances for bnaph and bbchrys range from 3.19-3.81 Å and 3.11-3.82 Å, respectively. The carbon atoms separated by the largest intermolecular distances are the ones on the end of the shorter continuous acene segment, which is one ring long for bnaph and two rings long for bbchrys.

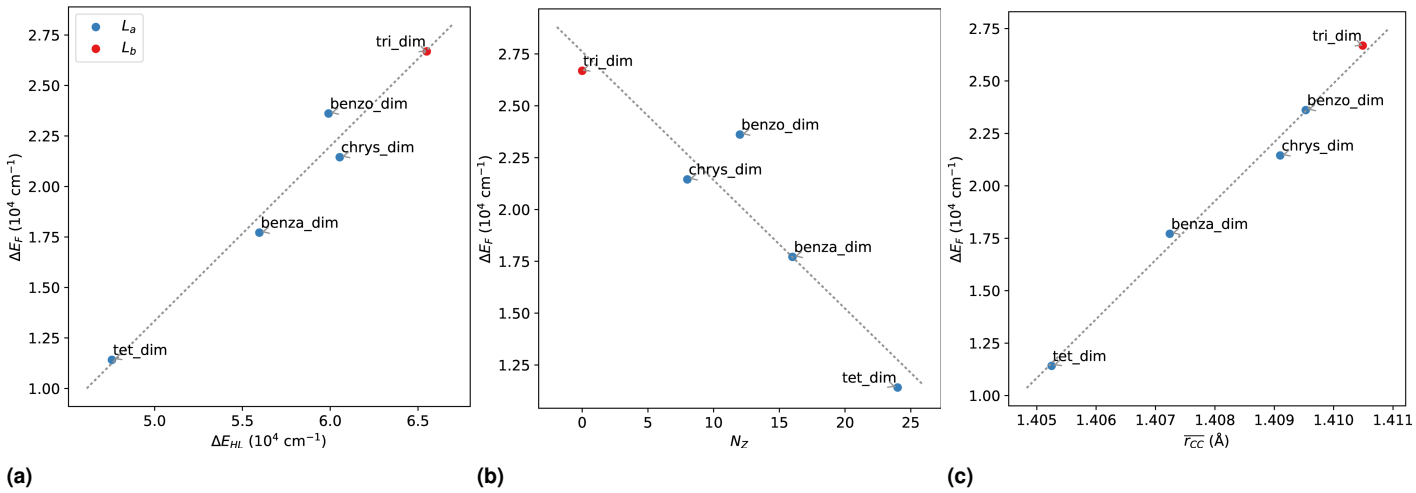

Fig. 2 Variation in ΔE_F for excimers containing tet isomers with respect to ΔE_{HL}, N_Z, and $\overline{r_{CC}}$.

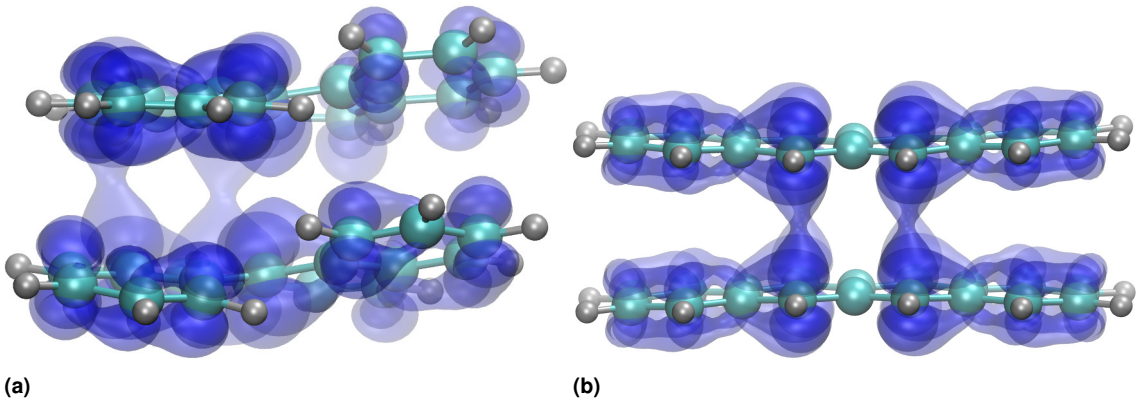

Fig. 3 Orbitals involved in the $S_0 \rightarrow S_1$ transition for the tet excimer (left) and the benzo excimer (right), with ± 0.03 isosurfaces shown.

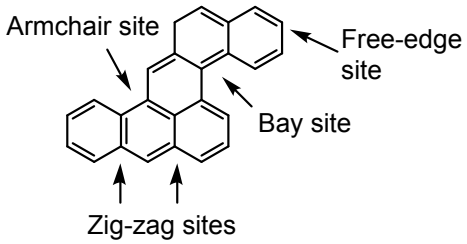

Fig. 4 PAH edge groups identified by Mosbach and coworkers.[54]

One isomer, dbphen, even includes a fjord group. As with benzo, the planar structure is distorted to prevent steric clashes between hydrogen atoms, with dihedral angles of approximately ± 17 ° for the carbon atoms in the fjord edge group. The dbphen excimer structure breaks the twofold symmetry of the dimer, leading to very large intermolecular C-C distances of up to ≈ 5.5 Å. This unexpected conformation means that ΔE_F is much higher than predicted by the simple N_Z descriptor. The ΔE_{HL} descriptor also underestimates ΔE_F, as was observed for the benzo excimer, which shares the dbphen excimer's twisted conformation.

In contrast, pentaph monomers have higher symmetry and are quite planar; the intermolecular C-C distances are 3.37-3.51 Å.

Table 1 Electronic properties for constituent monomers of the complexes considered in this work.

Monomer	Shortened name	Formula	ΔE_{HL} (cm^{-1})	Excitation type	ΔE_F (cm^{-1})
coronene	coro	$C_{24}H_{12}$	56997	L_b	26589
pyrene	pyr	$C_{16}H_{10}$	57178	L_b	30193
tetracene	tet	$C_{18}H_{12}$	47567	L_a	21983
benz[a]anthracene	benza	$C_{18}H_{12}$	55965	L_a	28450
benzo[c]phenanthrene	benzo	$C_{18}H_{12}$	59906	L_b	28935
benzene	benz	C_6H_6	87843	L_b	42845
naphthalene	naph	$C_{10}H_8$	67239	L_b	35549
phenanthrene	phen	$C_{14}H_{10}$	66162	L_b	31827
anthracene	anth	$C_{14}H_{10}$	54428	L_a	27397
benz[e]pyrene	benzepyr	$C_{20}H_{12}$	57374	L_b	29420
benz[a]pyrene	benzapyr	$C_{20}H_{12}$	51990	L_a	26667
fluoranthene	fluor	$C_{16}H_{10}$	58859	L_a	22784
triphenylene	tri	$C_{18}H_{12}$	65499	L_b	31466
chrysene	chrys	$C_{18}H_{12}$	60542	L_b	30093
dibenz[a,j]anthracene	dibenz	$C_{22}H_{14}$	56056	L_b	27739
benzo[b]triphenylene	bbtri	$C_{22}H_{14}$	56018	L_b	29257
benzo[b]chrysene	bbchrys	$C_{22}H_{14}$	52975	L_a	26462
benzo[a]naphthacene	bnaph	$C_{22}H_{14}$	47891	L_a	22957
pentacene	penta	$C_{22}H_{14}$	41668	L_a	18332
perylene	perl	$C_{20}H_{12}$	48924	L_a	23680
pentaphene	pentaph	$C_{22}H_{14}$	55289	L_b	26406
picene	pice	$C_{22}H_{14}$	59511	L_b	28902
benzo[g]chrysene	bgchrys	$C_{22}H_{14}$	57674	L_b	28563
dibenzo[c,g]phenanthrene	dbphen	$C_{22}H_{14}$	58548	L_b	26867

Even pice, which has the maximum number of bay groups possible, has a larger monomer planarity index. The length of even

Table 2 Electronic and geometric properties of noncovalent homodimers.

Monomer	Monomer planarity	Excitation type	ΔE_F (cm^{-1})
tet	0.070	L_a	11416
benza	0.053	L_a	17715
benzo	0.231	L_a	23987
coro	0.005	L_b	21608
anth	0.061	L_a	16303
naph	0.036	L_a	23719
benzepyr	0.027	L_a	21432
benzapyr	0.044	L_a	16152
pyr	0.027	L_a	20040
phen	0.008	L_b	26267
fluor	0.020	L_a	19406
tri	0.007	L_b	26688
chrys	0.081	L_a	21450
dibenz	0.052	L_a	18560
bbtri	0.047	L_b	17718
bbchrys	0.048	L_a	15891
bnaph	0.062	L_a	11752
penta	0.072	L_a	7365
perl	0.013	L_a	14128
pentaph	0.018	L_a	19566
pice	0.025	L_a	22558
benz	0.007	L_b	32862
bgchrys	0.331	L_a	21322
dbphen	0.5814	L_a	24820

Table 3 R^2 values for the complex descriptors.

Descriptor	Tet Isomers	Pent Isomers	Naph containing	All
$\overline{\Delta E_{HL}}$	0.967	0.935	0.742	0.783
$\overline{\Delta E_F}$	0.863	0.712	0.688	0.758
$\overline{D}$	0.774	0.482	0.183	0.539
N_O	–	–	–	0.328
N_Z	0.885	0.507	0.390	0.486
$\overline{r_{CC}}$	0.990	0.755	0.819	0.471
M	–	–	0.173	0.343

Table 4 Electronic and geometric properties of noncovalent heterodimers.

Larger monomer	Smaller monomer	Planarity large mon	Planarity small mon	Excitation type	ΔE_F (cm^{-1})
coro	pyr	0.021	0.013	L_b	24516
tet	benz	0.063	0.003	L_a	21299
naph	benz	0.006	0.005	L_b	33411
phen	benz	0.007	0.001	L_b	31230
coro	naph	0.017	0.010	L_b	26001
coro	phen	0.022	0.007	L_b	25094
pyr	naph	0.041	0.014	L_b	25214
fluor	naph	0.038	0.017	L_a	21358
fluor	anth	0.044	0.010	L_a	19384
phen	naph	0.031	0.029	L_a	24882
anth	phen	0.043	0.049	L_a	22676
pyr	phen	0.019	0.012	L_a	22873
chrys	naph	0.072	0.006	L_a	26504
benza	naph	0.023	0.026	L_a	21664
benzapyr	naph	0.071	0.013	L_a	22306
anth	naph	0.034	0.031	L_a	20653
anth	benz	0.037	0.004	L_a	26631
pyr	benz	0.009	0.001	L_b	29789
tet	naph	0.009	0.016	L_a	18192
tri	naph	0.016	0.004	L_a	28417
benza	anth	0.042	0.052	L_a	16981
pyr	anth	0.061	0.010	L_a	21160
fluor	benz	0.005	0.003	L_a	22046
coro	anth	0.038	0.022	L_a	22447
coro	benz	0.018	0.001	L_b	26364
perl	naph	0.040	0.017	L_a	21706

the shortest C-C distance decreases the extent of intermonomer orbital overlap, leading to a much higher ΔE_F than the geometry descriptors predict. This planarity may result from the relatively small, equal number of rings in each acene-like segment of the molecule. The tendency to undergo stabilizing distortion away from planar conformations tends to emerge for molecules containing one longer acene-like segment. Although nearly 70% of the variation in ΔE_F is attributable to its the linear relationship with N_Z, the value of D as a monomer descriptor has been lost with the increasing geometric complexity. R^2 for the relationship between D and ΔE_F is less than 0.5.

3.3 Exciplexes Containing Naphthalene

Next, we consider naph-containing homo- and heterodimers, allowing the mass and geometry of one of the monomers to vary. The naph monomer is generally expected to be present in relatively high concentrations in flames, and the small size allows examination of a number of complexes at reasonable computational cost. In some cases, more than one eclipsed configuration is possible. Because emissions from the global minimum configurations (illustrated in Fig. S2) are expected to dominate due to relaxation on the S_1 surface, additional local minimum S_1 geometries are not considered.

In place of ΔE_{HL}, we introduce the simple arithmetic mean of the HOMO-LUMO gap for the two monomers in each complex, $\overline{\Delta E_{HL}}$, which is equal to ΔE_{HL} for homodimers. $\overline{\Delta E_{HL}}$ may be used to predict ΔE_F within ≈ 3000 cm^{-1} In total, the variation in $\overline{\Delta E_{HL}}$ for the complexes accounts for 71% of the variation in ΔE_F. The remaining variation may be attributed to the specifics of each interaction, in particular the amount of constructive orbital overlap possible given the geometric differences of the two monomers and the magnitude of the noncovalent interaction between the two. The naph excimer has the lowest-energy emission relative to the overall trend, which is not surprising given the high symmetry and perfect overlap of the complex. At the other extreme, the naph-coro exciplex has the highest energy.

N_Z, the total number of bonds in zig-zag sites over both monomers, largely fails as a predictor of ΔE_F. When the number of rings is allowed to vary, the number of possible PAH monomers with equal numbers of bonds in zig-zag edge groups is high; naph, phen, fluor, and chrys each have four. The r_{CC} descriptor is more successful, with $R^2 = 0.81$. The largest deviation from this linear trend is observed for the naph-fluor exciplex, which is not surprising given the presence of aliphatic bonds in the fluor molecule linking the naph- and benz-like groups.

3.4 The Complete Excimer and Exciplex Database.

Now we allow both monomers to vary in mass and geometry. The heterodimer combinations chosen form a representative subset of the complexes that may be formed from the smallest PAHs, which are suggested to be present at higher concentration in flames based on kinetic estimates.[7]

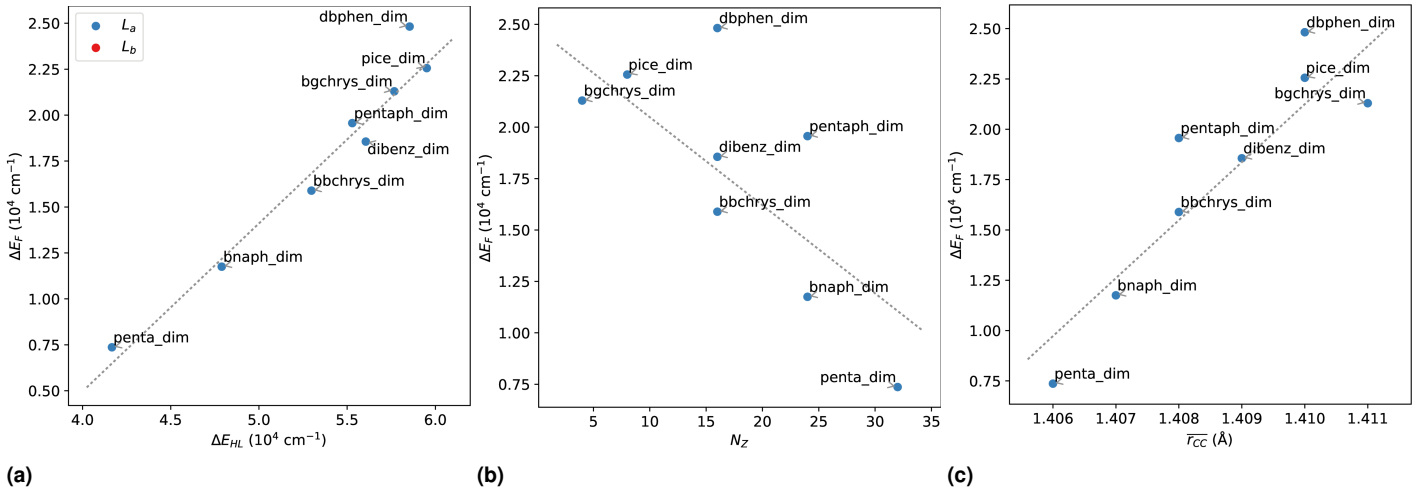

Fig. 5 Variation in ΔE_F for excimers containing pent isomers with respect to ΔE_{HL}, N_Z, and $\overline{r_{CC}}$.

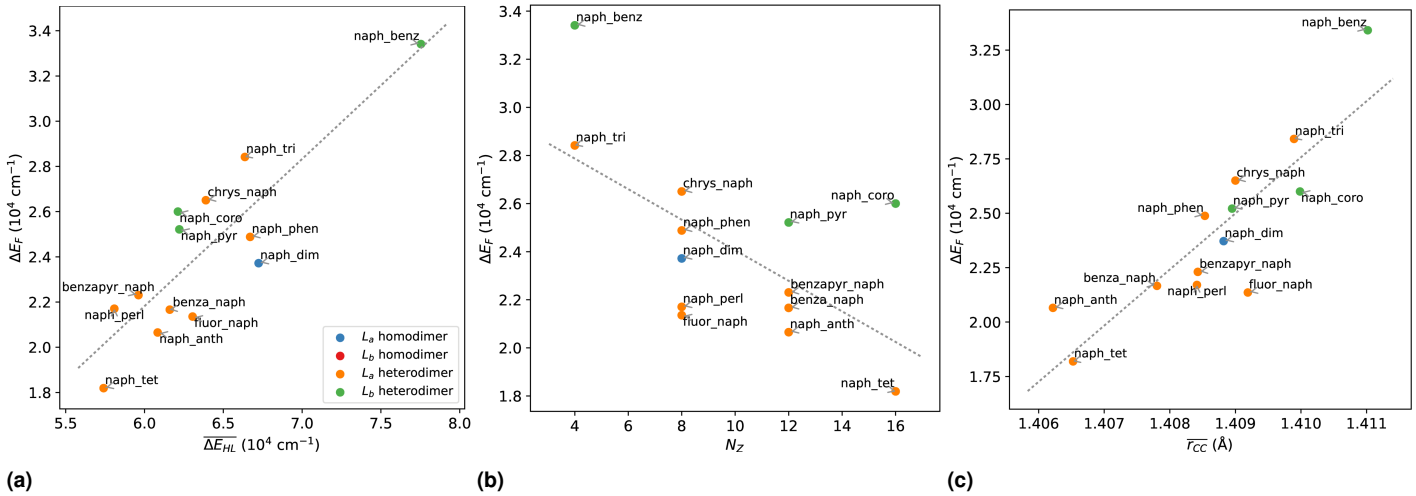

Fig. 6 Variation in ΔE_F for complexes containing naphthalene with respect to ΔE_{HL}, N_Z, and $\overline{r_{CC}}$.

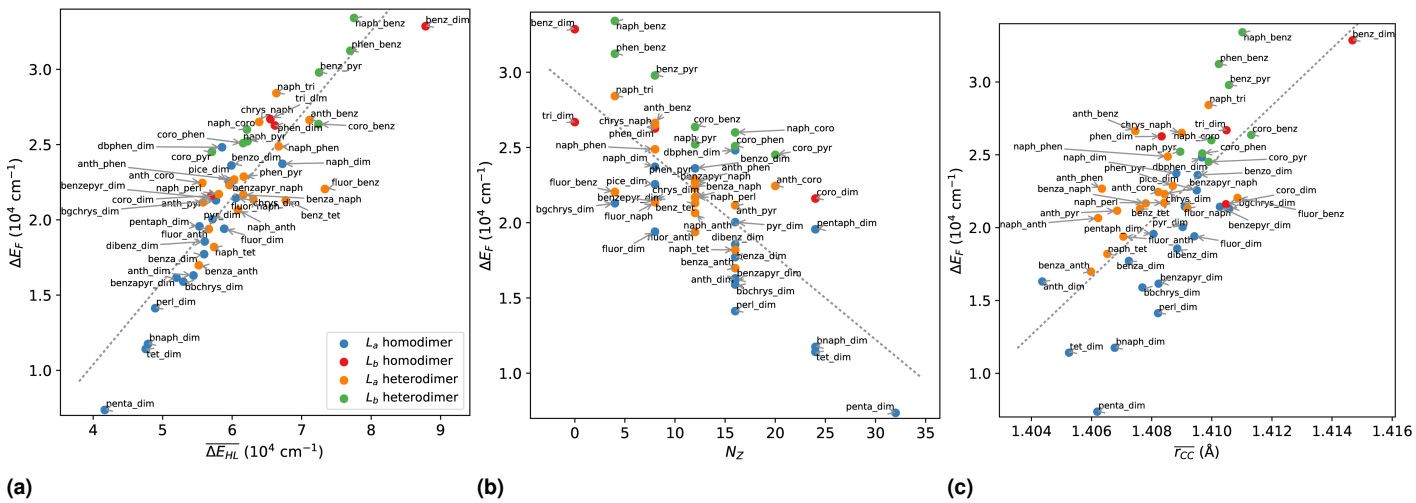

Fig. 7 Variation in ΔE_F for all complexes with respect to $\overline{\Delta E_{HL}}$, N_Z, and $\overline{r_{CC}}$.

The relationship between $\overline{\Delta E_{HL}}$ and ΔE_F holds surprisingly well, as Fig. 7a shows. This linear relationship explains approximately 80% of the variation in ΔE_F. The complexes emitting at the lowest energies relative to the overall trend are generally ho-

modimers; the benz dimer in particular has a ΔE_F approximately 5000 cm^{-1} lower than predicted from $\overline{\Delta E_{HL}}$. The coro-pyr dimer has the highest-energy emission compared to the predicted value. For heterodimers, the lowest-energy configuration typically has the smaller molecule centered over the larger molecule, minimizing the mean intermolecular C-C distance. This is not the case for the naph-coro, phen-coro, or anth-coro complexes, where the most favorable configurations avoid the central "hole," a ring that has neither an aromatic sextet nor double bonds. For pyr, avoiding overlap with the hole means that two pyr rings extend past the edge of the coro monomer, a geometry even less favorable than the centered one. This example illustrates the value of Clar structures in rationalizing E_F observations, even if sextet counts are not used in quantitative models. The most noticeable ΔE_F underestimates are observed for the benz-fluor and benz-tet complexes. Because the HOMO energy for benz is significantly higher than for either fluor or tet, the excitations remain localized on the larger chromophores, as has been observed for the benz-anth exciplex.[20]

For the complete database of complexes, the variation in ΔE_F associated with the geometric descriptors is again much lower than observed in each isomer group, with $R^2 = 0.49$ for the relationship between ΔE_F and N_Z. This is not surprising, given the broader array of PAH topologies present. The introduction of pericondensed molecules and the presence of heterodimers complicates the relationship between N_Z and PAH topology, with N_Z identical for complexes as electronically dissimilar as the chrys dimer and the benz-pyr complex. It is not clear whether including more edge group counts in the model would improve agreement—edge topology is, if anything, more diverse for the larger tet and pent isomers.

Considering the monomer-mass-weighted $\overline{r_{CC}}$ (Fig. 7c) does not improve the correlation coefficient—like N_Z, this relationship accounts for about 50% of the ΔE_F variation. Examining $\overline{r_{CC}}$ values also reveals an unexpected trend in excited-state monomer geometries. In general, ground-state C-C bond lengths increase with increasing PAH mass, but the longest S_1 $\overline{r_{CC}}$ is the one obtained for benz, with the shortest values obtained for anth and tet. In general, $\overline{r_{CC}}$ is longer for complexes with L_b $S_0 \rightarrow S_1$ transitions and shorter for complexes with L_a transitions. The arithmetic mean of the monomer diameters, $\overline{D}$, has similar predictive power, with $R^2 = 0.54$ for the linear relationship between $\overline{D}$ and ΔE_F.

Though the geometry-based models used here have limited predictive power, each is still more useful than a one-dimensional model based on total complex mass M, which accounts for only 34% of the variation in ΔE_F. This level of success for the M-based model is likely explained by the fact that linear acenes, which are overrepresented among small PAHs and thus overrepresented in this database, do have $\overline{\Delta E_{HL}}$ values that decrease with increasing mass. The wide variation of ΔE_F among tet isomers and among pent isomers shows that mass is often useless in predicting ΔE_F. Similarly, the number of intermonomer C-C pairs that directly overlap, N_O, which we define as being separated by a distance of < 0.25 Å in the plane of the monomers, has little predictive value, with $R^2 = 0.33$ for its linear relationship with ΔE_F.

3.5 Aliphatically-Bridged Complexes.

Finally, we examine the possibility that PAHs connected by aliphatic linkers could be the source of visible-range fluorescence. MD/metadynamics simulations suggest that aliphatically-bridged PAHs have lower homodimerization propensity than similarly-sized PAHs that do not contain sp3 carbons,[57] but intramolecular exciplex formation can occur without dimerization. Substitution with saturated hydrocarbon groups has a significant effect on the noncovalent dimerization propensity of PAHs,[9] but the effect on PAH monomer electronic structure is expected to be small.[58] However, because orbital overlap is so critical to the stabilizing exciplex interaction, we would expect that if the presence of the linker disrupted the eclipsed configuration of the PAH sufficiently, this stabilization would be eliminated. Maintaining the eclipsed configuration entails significant angle strain for the aliphatic linker. In a study of the conformations of benzene molecules with attached aliphatic chains, the aliphatic chain had to be at least eight carbons in length for a conformation with the chain folded on top of the benzene to be observed at 110 °C.[59] At flame temperature, a wide range of conformational states are likely to be accessible to vibrationally-excited linked complexes. Our goal is not to calculate the relative free energy of the eclipsed conformation, but simply to determine the effect of the linker on the minimum-energy sandwich-like excited state structure and on the fluorescence emission energy for that structure.

Considering all possible linker lengths and positions for every complex in our noncovalent database is beyond the scope of this work. Instead, we have chosen a representative subset of structures from across the spectrum: the benz excimer, the benz-naph exciplex, the naph-anth exciplex, and the naph and anth excimers. Bridged structures suggested to be consistent with recent tandem mass spectrometry results include linkers with one to four carbons,[34] but we have confined our survey to complexes with two-to-four carbon linkers, where excimer formation produces less angle strain. Linker attachment points at the endmost carbon (α position), one carbon closer to the molecule center of mass (β position), and two carbons closer to the center of mass (γ position) have been considered. In each case, the attachment point is the same for both molecules.

Fluorescence wavelengths of the linked structures are reported in Table 5 and Figure 8. Often, the effect of the covalent linker on ΔE_F is small, particularly for two- and four-C linkers. The linkers generally lower ΔE_F, with the strongest effect observed for C3 linkers. Examining the minimum-energy S_1 structures and frontier orbital isosurfaces obtained for the linked benz excimer (Fig. 9) reveals why this is the case. The C2 linker disrupts the parallel eclipsed structure of the monomers. Intermolecular C-C distances range from 2.54 Å for the Cs closest to the linker to 3.24 Å; the noncovalent excimer has C-C distances ranging from 2.96-2.98 Å. The C2 frontier orbitals (Fig. 9a) show reduced intermonomer electron density in the region with the largest C-C distances, farthest away from the linker. The similarity of the ΔE_F values obtained for the noncovalent and C2 structures is likely due in part to a partial delocalization of the orbitals involved in the transition (in particular the LUMO+1 orbital) over

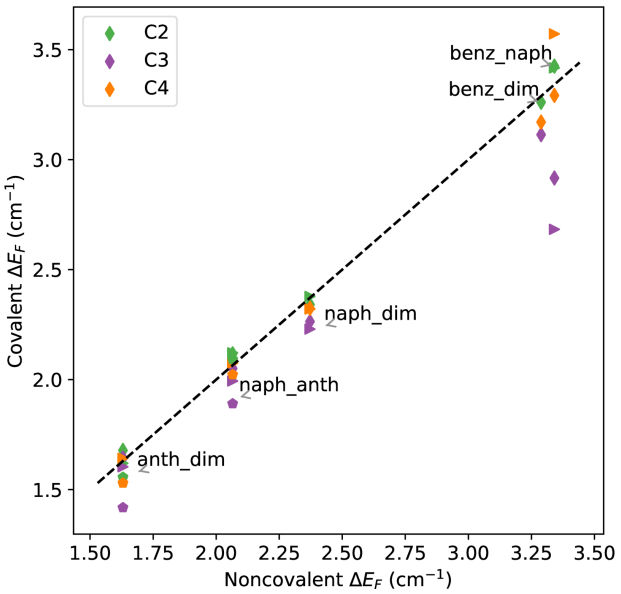

Fig. 8 Emission energies for aliphatically-bridged complexes vs. emission energies for the corresponding noncovalent complexes. Diamonds indicate linkers on α carbons, triangles indicate β carbons, and pentagons indicate γ carbons. A dotted $x = y$ curve has been added.

the linker carbons. Because we have calculated vertical fluorescence energies, it is also likely that the lower ΔE_F results in part from higher repulsion energy on the ground-state potential energy surface. Benz dimers with C3 and C4 linkers have nearly-intact eclipsed structures, with 2.80-3.14 Å C-C distances (Figs. 9b and 9c). The C3 structure has the slightly lower-energy emission and more extensive frontier orbital electron density delocalization over the linker. The one structure where the energetic impact of the aliphatic linker is significant is the benz-naph exciplex with a C3 linker in the β position. ΔE_F is lowered by nearly 7500 cm^{-1}. In this case, the eclipsed configuration is maintained, and the order of the two lowest-energy singlet excited states flips; the L_a state becomes lower in energy than the L_b state.

The range of energies obtained for each complex generally decreases in size as mass increases. For the naph dimer, the linker position has virtually no impact on ΔE_F. In contrast, ΔE_F for the anth dimer is noticeably decreased for linkers in the γ position. The optimal S_1 geometry for the anth dimer is already nonplanar, with the central carbons of the two molecules closest together (3.05 Å) and the end carbons farther apart (3.41 Å). This geometry is perturbed the least when the linker is bound to the central carbons.

Of course, ΔE_F is not the only aspect of the electronic transition affected by the addition of a linker. The oscillator strength for the fluorescence emission from most of the noncovalent homodimers is equal to zero for symmetry reasons (Tables S6). At flame temperature, intra- and intermolecular dimer modes are expected to be excited, resulting in nonzero oscillator strengths. The aliphatically-bridged structures, on the other hand, have nonzero oscillator strengths even in their minimum-energy S_1 geometries (Table S8). Changing the position or length of the linker can cause the oscillator strength to vary by two orders of magnitude.

Table 5 Emission wavelengths for covalently-linked structures.

Complex	Linker position	Linker length	Excitation type	ΔE_F (cm^{-1})
anth dimer	2	α	L_a	16972
	2	β	L_a	16200
	2	γ	L_a	15564
	3	α	L_a	16431
	4	β	L_a	16426
	3	γ	L_a	14184
	3	β	L_a	16038
	4	γ	L_a	15300
anth-naph complex	2	β	L_a	21222
	3	β	L_a	19936
	4	β	L_a	20747
	2	γ	L_a	20921
	3	γ	L_a	18907
	4	γ	L_a	20227
	2	α	L_a	21173
	3	α	L_a	20509
naph dimer	2	α	L_a	23414
	3	α	L_a	22640
	4	α	L_a	23240
	3	β	L_a	22297
	4	β	L_a	23629
	2	β	L_a	23781
benz-naph complex	2	α	L_b	34247
	3	α	L_a	29163
	2	β	L_b	34165
	3	β	L_a	26831
	4	β	L_a	35714
	4	α	L_a	30912
benz dimer	4	α	L_b	31706
	2	α	L_b	32605
	3	α	L_a	31133

4 Conclusions

In this work, we have demonstrated that many of the noncovalent and aliphatically-bridged complexes that can be formed from small to moderately-sized, flame-relevant PAHs have fluorescence emission energies in the visible range. The emission energy for complexes depends strongly on monomer topology. Within the sets of tetracene isomers and pentacene isomers, clear linear relationships exist between geometric characteristics such as the number of zig-zag edge groups and mean excited-state bond length and the excimer emission energy. Monomer HOMO-LUMO gap provides an excellent proxy for geometric effects on emission energy.

While the simple geometric models prove less predictive for a database of complexes containing both homo- and heterodimers, the linear relationship with the mean monomer HOMO-LUMO gap still accounts for almost 80% of the variation in complex emission energies. The value of this observation is clear: not only do polynomial-scaling computational costs for electronic structure methods make calculations of monomer properties significantly cheaper than dimer properties, but $\sim n^2$ complex fluorescence energies may be predicted from a database of n HOMO-LUMO gaps. It is important to note, though, that this model does not provide a means of distinguishing between complexes with similar mean HOMO-LUMO gaps on the basis of fluorescence emission energy. Complex-specific calculations will be required

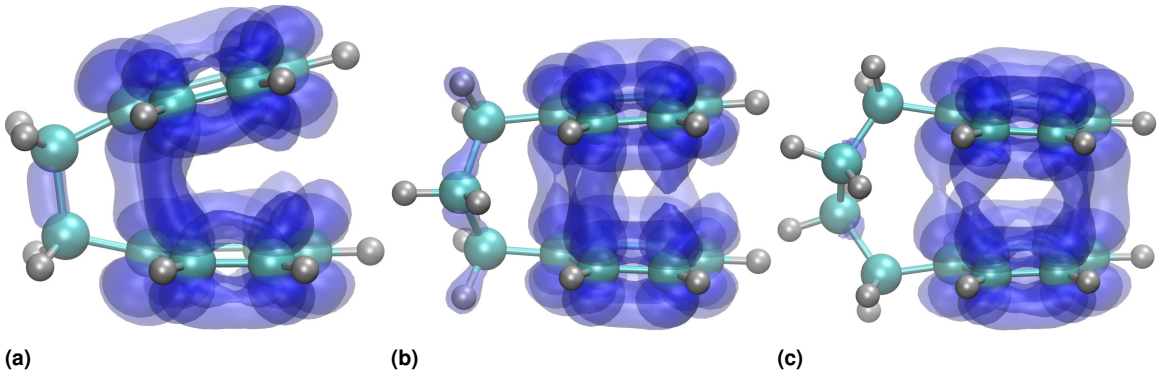

Fig. 9 Orbitals involved in the $S_0 \rightarrow S_1$ transition for aliphatically-bridged benz dimers, with ± 0.05 isosurfaces shown.

when an error of ≈ 3000 cm^{-1} is not acceptable.

Lastly, we have shown that the presence of aliphatic linkers does not significantly affect trends in fluorescence emission energies. The variation in fluorescence observed is the result of distortion of the minimum-energy noncovalent complex structure and also delocalization of the orbitals involved in the transition over the covalent linker. Distinguishing between noncovalent and bridged structures will require more detailed analysis of spectral features or a combination of experimental methods.

Conflicts of interest

"There are no conflicts to declare".

Acknowledgements

R. A. K. acknowledges funding from the NSF Division of Graduate Education (DGE-1745301)

Notes and references

1 Q. Di, Y. Wang, A. Zanobetti, Y. Wang, P. Koutrakis, C. Choirat, F. Dominici and J. D. Schwartz, *N. Engl. J. Med.*, 2017, **376**, 2513–2522.

2 K. R. Smith, N. Bruce, K. Balakrishnan, H. Adair-Rohani, J. Balmes, Z. Chafe, M. Dherani, H. D. Hosgood, S. Mehta, D. Pope and E. Rehfuess, *Annu. Rev. Public Health*, 2014, **35**, 185–206.

3 Y. Qian, W. I. Gustafson, L. R. Leung and S. J. Ghan, *J. Geophys. Res. Atmos.*, 2009, **114**, 1–19.

4 J. R. McConnell, R. Edwards, G. L. Kok, M. G. Flanner, C. S. Zender, E. S. Saltzman, J. R. Banta, D. R. Pasteris, M. M. Carter and J. D. W. Kahl, *Science (80-.).*, 2007, **317**, 1381–1385.

5 S. E. Stein and A. Fahr, *J. Phys. Chem.*, 1985, **89**, 3714–3725.

6 P. D. Teini, D. M. A. Karwat and A. Atreya, *Combust. Flame*, 2011, **158**, 2045–2055.

7 H. Wang, *Proc. Combust. Inst.*, 2011, **33**, 41–67.

8 Q. Mao, A. C. van Duin and K. H. Luo, *Carbon N. Y.*, 2017, **121**, 380–388.

9 P. Elvati and A. Violi, *Proc. Combust. Inst.*, 2013, **34**, 1837–1843.

10 T. S. Totton, A. J. Misquitta and M. Kraft, *Phys. Chem. Chem. Phys.*, 2012, **14**, 4081–94.

11 H. A. Michelsen, *Proc. Combust. Inst.*, 2017, **36**, 717–735.

12 E. M. Adkins and J. H. Miller, *Phys. Chem. Chem. Phys.*, 2015, **17**, 2686–2695.

13 X. Mercier, O. Carrivain, C. Irimiea, A. Faccinetto and E. Therssen, *Phys. Chem. Chem. Phys.*, 2019, 1–37.

14 J. H. Miller, *Proc. Combust. Inst.*, 2005, **30**, 1381–1388.

15 J. B. Birks, *Photophysics of Aromatic Molecules*, Wiley – Interscience, New York, 1970.

16 T. Takaya, C. Su, K. de La Harpe, C. E. Crespo-Hernandez and B. Kohler, *Proc. Natl. Acad. Sci.*, 2008, **105**, 10285–10290.

17 J. Xia, S. N. Sanders, W. Cheng, J. Z. Low, J. Liu, L. M. Campos and T. Sun, *Adv. Mater.*, 2017, **29**, 1601652.

18 D. Casanova, *J. Chem. Theory Comput.*, 2015, **11**, 2642–2650.

19 S. Shirai, Y. Kurashige and T. Yanai, *J. Chem. Theory Comput.*, 2016, **12**, 2366–2372.

20 R. A. Krueger and G. Blanquart, *J. Phys. Chem. A*, 2019, **123**, 1796–1806.

21 R. A. Krueger and G. Blanquart, *Int. J. Quantum Chem.*, 2019, **119**, e25819.

22 K. Diri and A. I. Krylov, *J. Phys. Chem. A*, 2012, **116**, 653–662.

23 J. Hoche, H.-c. Schmitt, A. Humeniuk, I. Fischer and M. I. S. Ro, *Phys. Chem. Chem. Phys.*, 2017, **19**, 25002–25015.

24 R. Huenerbein and S. Grimme, *Chem. Phys.*, 2008, **343**, 362–371.

25 M. Kołaski, C. R. Arunkumar and K. S. Kim, *J. Chem. Theory Comput.*, 2013, **9**, 847–856.

26 S. Shirai, S. Iwata, T. Tani and S. Inagaki, *J. Phys. Chem. A*, 2011, **115**, 7687–7699.

27 E. M. Adkins, J. A. Giaccai and J. H. Miller, *Proc. Combust. Inst.*, 2017, **36**, 957–964.

28 M. R. Kholghy, G. A. Kelesidis and S. Pratsinis, *Phys. Chem. Chem. Phys.*, 2018, **20**, 10926–10938.

29 M. Kasha, *Disc. Faraday Soc*, 1950, **9**, 9–14.

30 E. M. Adkins and J. H. Miller, *Phys. Chem. Chem. Phys.*, 2017, **19**, 28458–28469.

31 Y. Ruiz-Morales, *J. Phys. Chem. A*, 2002, **106**, 11283–11308.

32 Y.-C. Chang, M.-Y. Kuo, C.-P. Chen, H.-F. Lu and I. Chao, *J. Phys. Chem. C*, 2010, **114**, 11595–11601.

33 K. O. Johansson, M. P. Head-Gordon, P. E. Schrader, K. R. Wil-

son and H. A. Michelsen, *Science (80-.).*, 2018, **1000**, 997–1000.

34 B. D. Adamson, S. A. Skeen, M. Ahmed and N. Hansen, *J. Phys. Chem. A*, 2018, acs.jpca.8b08947.

35 F. Plasser and H. Lischka, *J. Chem. Theory Comput.*, 2012, **8**, 2777–2789.

36 A. Prlj, M. E. Sandoval-Salinas, D. Casanova, D. Jacquemin and C. Corminboeuf, *J. Chem. Theory Comput.*, 2016, **12**, 2652–2660.

37 S. Grimme and M. Parac, *Chemphyschem*, 2003, **4**, 292–295.

38 T. Leininger, H. Stoll, H.-J. Werner and A. Savin, *Chem. Phys. Lett.*, 1997, **275**, 151–160.

39 N. Kuritz, T. Stein, R. Baer and L. Kronik, *J. Chem. Theory Comput.*, 2011, **7**, 2408–2415.

40 T. Stein, L. Kronik and R. Baer, *J. Am. Chem. Soc.*, 2009, **131**, 2818–2820.

41 S. Grimme, *J. Chem. Phys.*, 2006, **124**, 034108.

42 M. Head-Gordon, R. J. Rico, M. Oumi and T. J. Lee, *Chem. Phys. Lett.*, 1994, **219**, 21–29.

43 M. Caricato, G. W. Trucks, M. J. Frisch and K. B. Wiberg, *J. Chem. Theory Comput.*, 2011, **7**, 456—-466.

44 Z. C. Wong, W. Y. Fan, T. S. Chwee and M. B. Sullivan, *Phys. Chem. Chem. Phys.*, 2017, **19**, 21046–21057.

45 F. Weigend and R. Ahlrichs, *Phys. Chem. Chem. Phys.*, 2005, **7**, 3297–3305.

46 A. D. Laurent, A. Blondel and D. Jacquemin, *Theor. Chem. Acc.*, 2015, **134**, 1–11.

47 F. Neese, *Wiley Inderdiscip. Rev. Comput. Mol. Sci.*, 2012, **2**, 73–78.

48 E. S. S. Iyer, A. Sadybekov, O. Lioubashevski, A. I. Krylov and S. Ruhman, *J. Phys. Chem. A*, 2017, **121**, 1962–1975.

49 N. O. Dubinets, A. A. Safonov and A. A. Bagaturyants, *J. Phys. Chem. A*, 2016, **120**, 2779–2782.

50 D. Casanova, *Int. J. Quantum Chem.*, 2015, **115**, 442–452.

51 NIST, *The NIST Polycyclic Aromatic Hydrocarbon Structure Index*, http://pah.nist.gov.

52 E. Clar, *Polycyclic Hydrocarbons*, Springer Berlin Heidelberg, Germany, 1964.

53 M. Antić, B. Furtula and S. Radenković, *J. Phys. Chem. A*, 2017, **121**, 3616–3626.

54 S. Mosbach, M. S. Celnik, A. Raj, M. Kraft, H. R. Zhang, S. Kubo and K. O. Kim, *Combust. Flame*, 2009, **156**, 1156–1165.

55 R. C. Fortenberry, C. M. Novak, T. J. Lee, P. P. Bera and J. E. Rice, *ACS Omega*, 2018, **3**, 16035–16039.

56 L. Jones and L. Lin, *J. Phys. Chem. A*, 2017, **121**, 2804–2813.

57 P. Elvati, K. Turrentine and A. Violi, *Proc. Combust. Inst.*, 2017, **37**, 1099–1105.

58 D. Chen and H. Wang, *Proc. Combust. Inst.*, 2018, **37**, 953–959.

59 D. M. Hewett, S. Bocklitz, D. P. Tabor, E. L. Sibert, M. A. Suhm and T. S. Zwier, *Chem. Sci.*, 2017, **8**, 5305–5318.

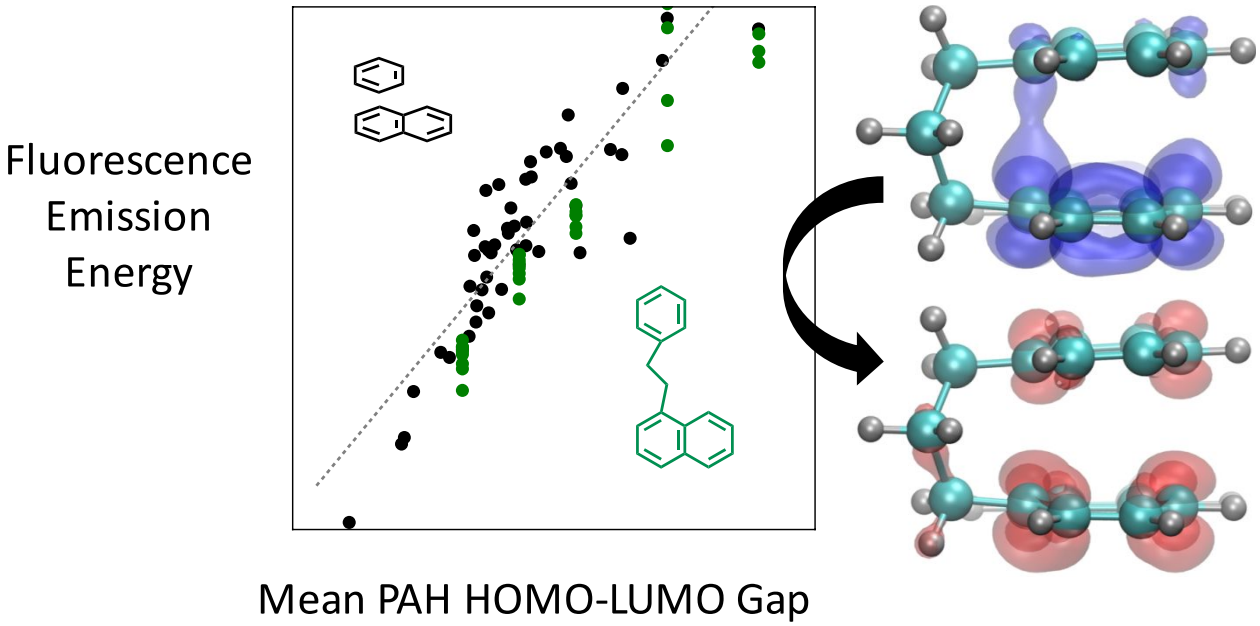

Analysis of PAH exciplex TDDFT fluorescence energies shows a linear relationship between mean monomer HOMO-LUMO gap and complex fluorescence.